Structural Engineering and Mechanics, *Vol. 63, No. 6 (2017) 809-824*
DOI: https://doi.org/10.12989/sem.2017.63.6.809

Analysis and probabilistic modeling of wind characteristics of an arch bridge using structural health monitoring data during typhoons

X.W. Ye*, P.S. Xi[a], Y.H. Su[b] and B. Chen[b]

Department of Civil Engineering, Zhejiang University, Hangzhou 310058, China

(Received October 19, 2016, Revised March 17, 2017, Accepted June 5, 2017)

Abstract. The accurate evaluation of wind characteristics and wind-induced structural responses during a typhoon is of significant importance for bridge design and safety assessment. This paper presents an expectation maximization (EM) algorithm-based angular-linear approach for probabilistic modeling of field-measured wind characteristics. The proposed method has been applied to model the wind speed and direction data during typhoons recorded by the structural health monitoring (SHM) system instrumented on the arch Jiubao Bridge located in Hangzhou, China. In the summer of 2015, three typhoons, i.e., Typhoon Chan-hom, Typhoon Soudelor and Typhoon Goni, made landfall in the east of China and then struck the Jiubao Bridge. By analyzing the wind monitoring data such as the wind speed and direction measured by three anemometers during typhoons, the wind characteristics during typhoons are derived, including the average wind speed and direction, turbulence intensity, gust factor, turbulence integral scale, and power spectral density (PSD). An EM algorithm-based angular-linear modeling approach is proposed for modeling the joint distribution of the wind speed and direction. For the marginal distribution of the wind speed, the finite mixture of two-parameter Weibull distribution is employed, and the finite mixture of von Mises distribution is used to represent the wind direction. The parameters of each distribution model are estimated by use of the EM algorithm, and the optimal model is determined by the values of R^2 statistic and the Akaike's information criterion (AIC). The results indicate that the stochastic properties of the wind field around the bridge site during typhoons are effectively characterized by the proposed EM algorithm-based angular-linear modeling approach. The formulated joint distribution of the wind speed and direction can serve as a solid foundation for the purpose of accurately evaluating the typhoon-induced fatigue damage of long-span bridges.

Keywords: structural health monitoring; wind characteristics; typhoon; joint distribution function; angular-linear approach; expectation maximization algorithm

1. Introduction

Recently, a considerable number of large-scale landmark bridges have been built in China. As the bridge span increases, the sensitivity of long-span bridges to random wind excitations will be significant (Ge and Xiang 2008, Li *et al.* 2008, Cheng and Li 2009, Cai *et al.* 2015). In 1940, the Tacoma Narrows Bridge was destroyed by the wind-induced flutter and this accident made the government and researchers aware of the wind effects on bridges. Thus, the acquaintance of the structural behaviors of bridges in the extreme environments should be of prime importance in the stages of structural design and condition assessment, especially for the long-span bridges located in the areas influenced by typhoons. Up to now, some studies were carried out to evaluate the wind- induced fatigue damage of bridges considering the typhoon effect (Gu *et al.* 1999, Xu *et al.* 2009). There is no doubt that field measurement/ monitoring of wind characteristics around the bridge can provide the most realistic and effective information for accurate evaluation of the wind-induced structural responses under the extreme environment (Li *et al.* 2002). However, because of the insufficiency of reliable in-situ wind data, most previous investigations still employ the wind data measured by the meteorological observatory away from the bridge site.

In the past three decades, the structural health monitoring (SHM) technology has gained increasingly attentions from the civil engineering community. Many SHM systems have been designed and implemented on large-scale bridges to continuously monitor the real-time environmental and traffic excitations as well as the structural responses (Ni *et al.* 2010, Lei *et al.* 2012, Ni *et al.* 2012, Ye *et al.* 2012, Ye *et al.* 2013, Ye *et al.* 2014, Lei *et al.* 2015, Ye *et al.* 2015, Ding *et al.* 2016, Ye *et al.* 2016a, b, c, d, Ding *et al.* 2017). Since the wind characteristics are closely associated with the local geography and climate, the field wind monitoring data obtained from the SHM system instrumented on the bridge are capable of offering crucial information for the examination of the wind-induced structural vibration and safety status. In recent years, many investigators have conducted the research of data-driven structural integrity, durability and reliability analysis using the long-term monitoring data of wind loads and wind effects (Xu *et al.* 2000). For instance, Bietry *et al.* (1995)

*Corresponding author, Associate Professor
E-mail: cexwye@zju.edu.cn
[a]Msc Student
[b]Ph.D. Student

Copyright © 2017 Techno-Press, Ltd.

ISSN: 1225-4568 (Print), 1598-6217 (Online)

induced acceleration of the Saint-Nazaire cable-stayed bridge. Comanducci *et al.* (2015) addressed the use of natural frequency tracking and tools of multivariate statistical analysis for monitoring the structural condition of a suspension bridge under changing wind speed. In addition, some researchers investigated the nonstationary characteristics of wind records during typhoon events (Xu and Chen 2004).

It has been a hot research issue to predict the aerodynamic characteristics of the bridge under the action of wind loading, and the prerequisite for fulfilling this task is to accurately represent the stochastic wind characteristics, i.e., wind speed and wind direction, at the bridge site. It is not easy to solve because the wind speeds at different directions are varying and the wind speed is mutually related with the wind direction. As a consequence, it is favorable to characterize the wind characteristics from a probabilistic perspective (Li *et al.* 2013, Yan *et al.* 2013). Research efforts have been devoted to modeling of wind characteristics using the probability density function (PDF) of the wind speed and wind direction (Qu and Shi 2010, Alduse *et al.* 2015). A pioneering work is carried out by Johnson and Wehrly (1978), who proposed a method to produce the angular-linear distributions with each marginal distribution of the wind speed and wind direction. Carta *et al.* (2008a) presented a joint PDF by using angular-linear approach for wind energy analysis. Coles and Walshaw (1994) taken account of the directional behavior of the wind and constructed the joint probability distribution model of extreme wind speed and direction which includes the correlation of speed and direction. Ge and Xiang (2002) built the probability distribution model of extreme values and statistically analyzed the joint distribution of wind speed and corresponding direction. Qu and Shi (2010) adopted the Farlie-Gumbel-Morgenstern approach to construct the joint distribution function based on the univariate cumulative distribution function (CDF). Erdem and Shi (2011) presented a study of three bivariate distribution construction approaches and compare them by using the adjusted R^2 and root mean square error (RMSE).

This study presents the analysis and probabilistic modeling of wind characteristics during typhoons by use of the long-term wind monitoring data acquired by the anemometers installed on the arch Jiubao Bridge located in Hangzhou, China. This bridge has been instrumented with a long-term SHM system including three anemometers for wind loading monitoring. In this study, the monitoring data of three typhoons in 2015, i.e., Typhoon Chan-hom, Typhoon Soudelor and Typhoon Goni are employed to analyze the wind characteristics including the average wind speed and direction, wind rose diagram, wind turbulence intensity, gust factor, turbulence integral scale, and power density spectra of fluctuating wind speed. Moreover, in order to precisely describe the distribution characteristics of typhoon wind field, the angular-linear approach is applied to formulate the joint distribution of wind speed and direction with specified marginal distributions. For the marginal distribution of wind direction, the mixture of von Mises distribution is used to characterize the marginal distribution of wind direction due to its multimodal feature, and the mixture of Weibull distribution is used to represent the marginal distribution of wind speed. Furthermore, the model parameters are estimated by use of the expectation maximization (EM) algorithm and the choice of the optimal distribution model is judged by the values of R^2 statistic and Akaike's information criterion (AIC).

2. Long-term SHM system and wind monitoring data during typhoons

2.1 Description of Jiubao Bridge

The Jiubao Bridge, as illustrated in Fig. 1, is a long-span continuous steel-concrete composite arch bridge located in Hangzhou, China. Its total length is 1,855 m with a main span of 630 m (3×210 m). The girder and arch combination structure is employed in the main span of the bridge which contains three spans of the steel arch composite structure. The south approach spans (90 m+9×58 m+55 m) and the north approach spans (55 m+2×58 m+90 m) are made up of continuous constant cross-sectional reinforced concrete box girders. Fig. 2 shows the geographic location of the Jiubao Bridge (Google Maps 2016). It can be seen from Fig. 2 that the bridge serves as an important transportation hub crossing the Qiantang River and connects Xiaoshan and Jianggan districts of Hangzhou city from south to north. The bridge was opened to traffic in July 2012 and the design velocity of the vehicle is set to be 80 km/h.

According to the meteorological survey, the climate of the bridge site belongs to a humid subtropical climate with four distinctive seasons. More specifically, it experiences a long, very hot and humid summer and a chilly, cloudy and drier winter. In the summer, the bridge is usually suffered

Fig. 1 Jiubao Bridge

Fig. 2 Location of Jiubao Bridge (Google Maps 2016)

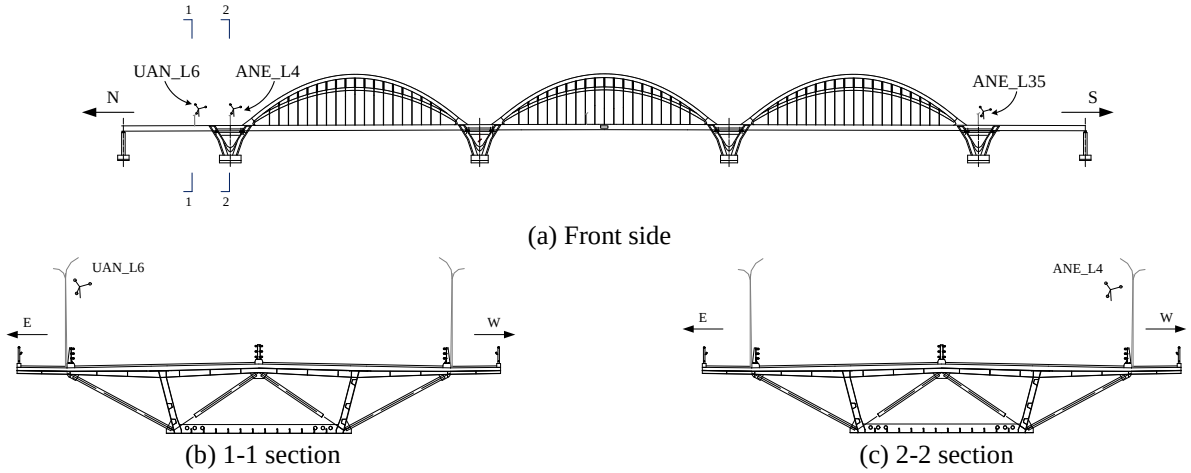

Fig. 3 Layout of anemometers on Jiubao Bridge

from several typhoon storms, while these typhoons seldom attack the bridge site directly. In general, they make landfall along the southern coast of Zhejiang Province and affect the bridge site with strong wind and heavy rainfall. For the sake of recognizing the dynamic behaviors and performances of the bridge in a strong wind environment, it is necessary to comprehensively examine the wind characteristics during typhoons to facilitate the analysis and computation of wind-resistant stability of the bridge.

2.2 SHM system and layout of anemometers

In order to assure the safety of the Jiubao Bridge, an SHM system has been installed on the bridge to monitor the integrity, durability and reliability of the bridge during the operation period. The system includes a total of 331 sensors divided into nine groups, namely anemometers, environmental temperature sensors, weigh-in-motion (WIM) sensors, vibration sensors, structural temperature sensors, strain gauges, level sensors, displacement sensors and cable tension sensors. These sensors are permanently deployed on the bridge and continuously collect the monitoring data reflecting the bridge health and safety condition.

The wind speed and wind direction data were simultaneously and continuously collected by two kinds of anemometers installed on the Jiubao Bridge. These anemometers include two mechanical anemometers and one ultrasonic anemometer. As illustrated in Fig. 3, two mechanical anemometers, named ANE_L4 and ANE_L35, were installed on the north side and south side of the main span deck respectively, and an ultrasonic anemometer, named UAN_L6, was installed on the north side of the bridge. All of these anemometers are deployed approximately 6 m high above the level of the bridge deck. The sampling frequency of the ultrasonic anemometer is set as 4 Hz and the sampling frequency of the mechanical anemometer is set as 0.1 Hz. The ultrasonic anemometer is able to detect the wind speed ranging from 0 to 60 m/s with an error within 0.01 m/s and the wind direction ranging from 0 to 360° with an error within 0.1°; while the mechanical anemometer can measure the wind speed ranging from 0 to 45 m/s with an error within 0.1 m/s and the wind direction ranging from 0 to 360° with an error within 0.1°. The wind direction angle 0° denotes north and 90° denotes east, rotating in a clockwise direction.

2.3 Monitoring data during three recorded typhoons

In this study, the wind monitoring data during three typhoons in 2015, i.e., Typhoon Chan-hom, Typhoon Soudelor and Typhoon Goni are extracted from the data management center of the instrumented long-term SHM system for further analysis. Typhoon Chan-hom is a large and long-lived tropical cyclone that affected most countries in the western Pacific basin. It was developed on 29 June 2015 from a westerly wind burst and moved to the northwest. Late from 9 July 2015 to 10 July 2015, it passed Okinawa and reached its peak wind speed of 165 km/h. It became the strongest typhoon to make landfall in Zhejiang Province at 16:40 on 11 July 2015 with an estimated wind speed of 150 km/h. Finally, it struck the North Korea and became an extratropical cyclone shortly thereafter. Fig. 4 illustrates the track of Typhoon Chan-hom (Japan Meteorological Agency 2015) and the location of Jiubao Bridge. As a typical wind data sample, Fig. 5 shows the measured wind data recorded by the ultrasonic anemometer UAN_L6 on 11 July 2015 during Typhoon Chan-hom.

Typhoon Soudelor is the strongest tropical cyclone of the Pacific typhoon season in 2015 and was formed as a tropical depression near Pohnpei on 29 July 2015. Then, it was further deepened and reached its peak intensity with a 10-minute maximum sustained wind speed of 215 km/h on 3 August 2015. On 7 August 2015, it was intensified to reach a secondary peak and later that day, it made landfall over Xiulin, Hualien in Taiwan at 04:40 on 8 August 2015. Around 22:10 on the same day, it made landfall over Putian, Fujian in China and the strongest gust was 191 km/h. The gale-force winds were extended into Jiangxi and Zhejiang provinces and affected wide areas of East China. Fig. 6 shows the historical route of Typhoon Soudelor (Japan Meteorological Agency 2015) and the location of Jiubao Bridge. Fig. 7 illustrates the recorded wind data measured by the ultrasonic anemometer UAN_L6 on 9 August 2015

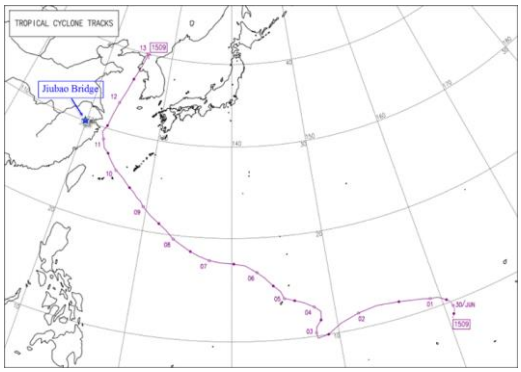

Fig. 4 Track of Typhoon Chan-hom (Japan Meteorological Agency 2015)

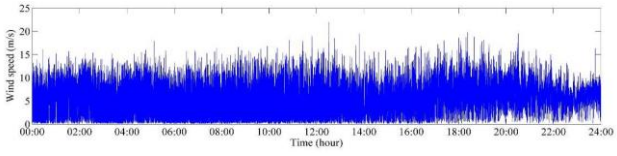

(a) Wind speed time histories

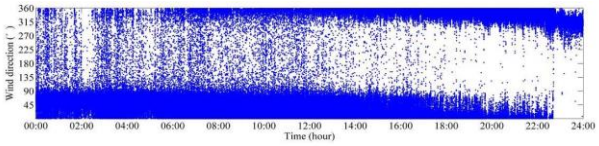

(b) Wind direction time histories

Fig. 5 Measured wind data of Typhoon Chan-hom

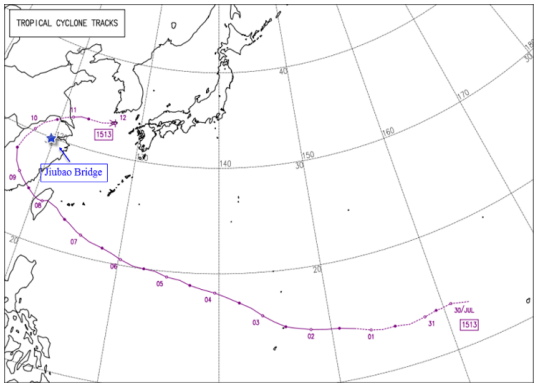

Fig. 6 Track of Typhoon Soudelor (Japan Meteorological Agency 2015)

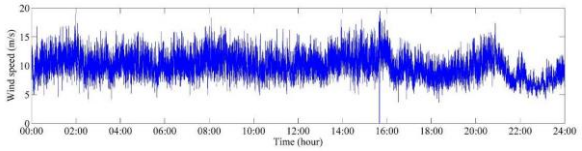

(a) Wind speed time histories

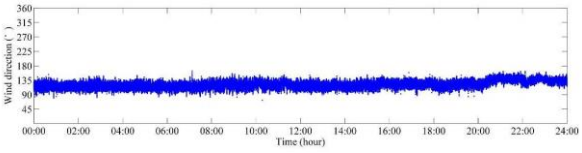

(b) Wind direction time histories

Fig. 7 Measured wind data of Typhoon Soudelor

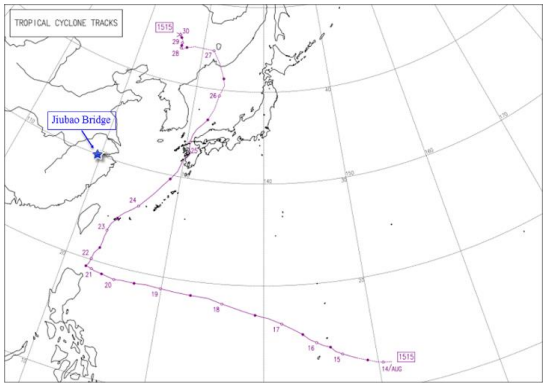

Fig. 8 Track of Typhoon Goni (Japan Meteorological Agency 2015)

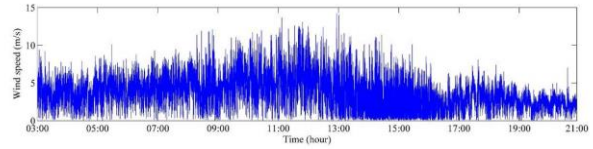

(a) Wind speed time histories

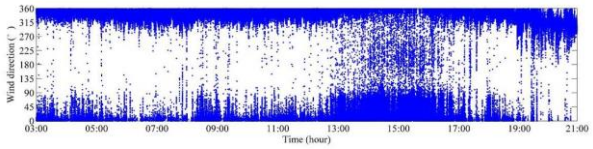

(b) Wind direction time histories

Fig. 9 Measured wind data of Typhoon Goni

during Typhoon Soudelor.

Typhoon Goni is a strong tropical cyclone that impacted many countries during late August 2015 and was intensified into a tropical depression on 13 August 2015. In the night of 15 August 2015, the Japan Meteorological Agency upgraded Goni to a severe tropical storm, and by the next day, it was intensified into a typhoon. Early on 17 August 2015, it was underwent rapid intensification and upgraded rapidly to a Category 4 typhoon and reached its first peak intensity. It quickly passed through Uki, Kumamoto after 20:00 and made landfall over Arao, Kumamoto after 21:00 on 24 August 2015. Then, it moved northeast and was transitioned into an extratropical cyclone and later affected Northeast China. Fig. 8 shows the historical track of the Typhoon Goni (Japan Meteorological Agency 2015) and the location of Jiubao Bridge. The wind data measured by the ultrasonic anemometer UAN_L6 during the period from 03:00 to 21:00 on 24 August 2015 during Typhoon Goni is illustrated in Fig. 9.

3. Analysis of wind characteristics during typhoons

3.1 Average wind speed and direction

In this section, the wind monitoring data recorded by the two anemometers, i.e., ultrasonic anemometer UAN_L6 and mechanical anemometer ANE_L35, are used to analyze the average wind characteristics and turbulence wind characteristics. The measured wind data includes the wind

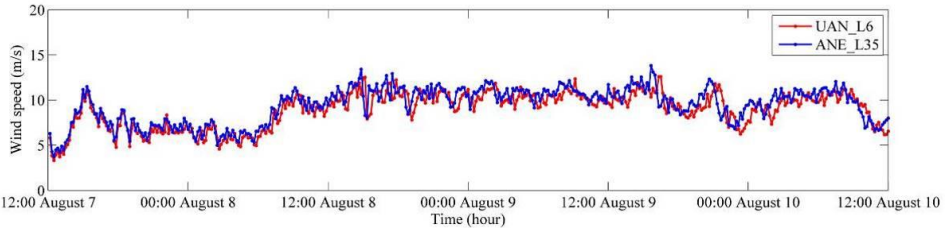

(a) Time histories of average wind speed

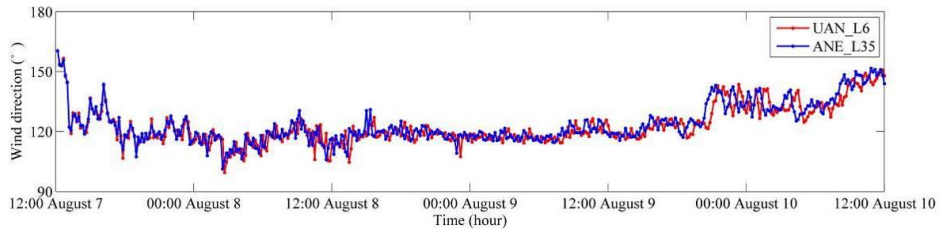

(b) Time histories of average wind direction

Fig. 10 Average wind speed and direction data of Typhoon Soudelor

speed $v(t)$ and the horizontal wind direction $\theta(t)$. In the analysis of the average wind, the basic interval for the average wind speed is 10 minutes. The average horizontal wind speed U and average wind direction ϕ in the 10-min interval are calculated by (Chen *et al.* 2013)

$$U = \sqrt{\bar{u}_x^2 + \bar{u}_y^2} \tag{1}$$

$$\cos\phi = \frac{\bar{u}_x}{U} \tag{2}$$

where $\bar{u}_x$ and $\bar{u}_y$ are the mean value of the wind speed time series $u_x(t)$ and $u_y(t)$, respectively. In the 10-min interval, the fluctuating longitudinal wind speed $u_x(t)$ and the fluctuating lateral wind speed $u_y(t)$ can be determined by

$$u(t) = u_x(t)\cos\phi + u_y(t)\sin\phi - U \tag{3}$$

$$v(t) = -u_x(t)\sin\phi + u_y(t)\cos\phi \tag{4}$$

The average wind speed and direction time histories (from 7 August 2015 to 10 August 2015) of Typhoon Soudelor for these two anemometers (UAN_L6 and ANE_L35) are illustrated in Fig. 10(a) and Fig. 10(b), respectively. It is observed from Fig. 10(a) and Fig. 10(b) that the characteristics of the mean wind speed and direction for these two kinds of anemometers are very similar. Fig. 10(a) shows that the 10-min average wind speeds during Typhoon Soudelor at the bridge site are ranged from 5 m/s to 15 m/s. The maximum 10-min average wind speeds measured by the mechanical anemometer and the ultrasonic anemometer are 13.82 m/s and 12.59 m/s, respectively. As illustrated in Fig 10(b), the wind direction time series indicate that the mean wind directions during Typhoon Soudelor are relatively steady ranging from 100° to 150°. The wind rose diagrams of average wind direction and the maximum mean wind speed in sixteen directions during Typhoon Soudelor are shown in Fig. 11. It can be found from Fig. 11 that the strong wind recorded by the ultrasonic anemometer (UAN_L6) is

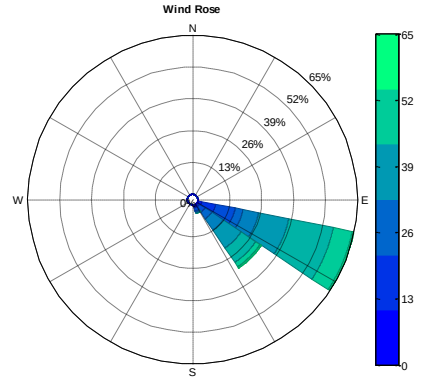

(a) Average wind direction

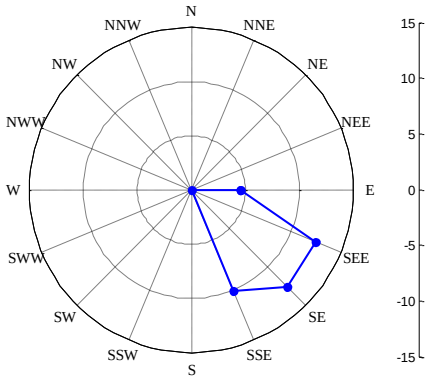

(b) Maximum average wind speed

Fig. 11 Wind rose diagram of Typhoon Soudelor

predominantly sourced from Southeast direction, and the maximum 10-min average wind speed reaches 12.59 m/s with the wind direction being SE.

3.2 Turbulence intensity and gust factor

The turbulence intensity is one of the most important components which can reflect the turbulence characteristic of the strong wind. After calculating the fluctuating wind speed and the average wind speed, the turbulence intensity

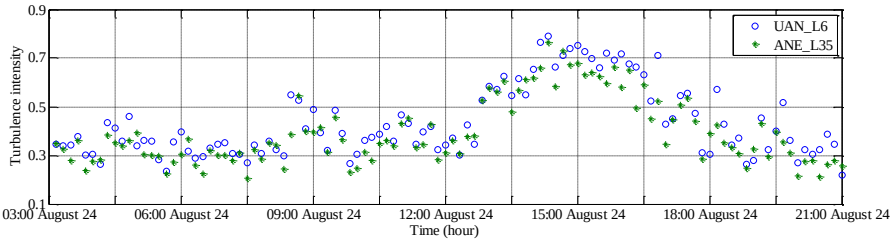

(a) Longitudinal direction

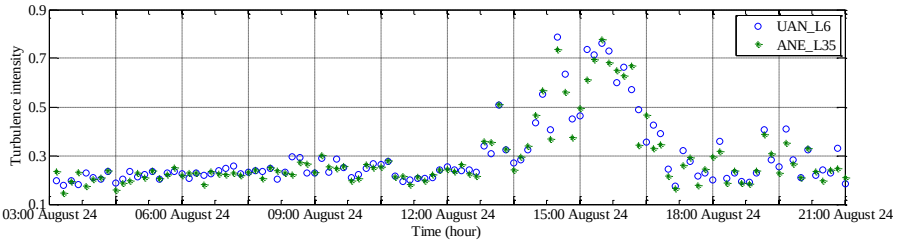

(b) Lateral direction

Fig. 12 Turbulence intensity of Typhoon Goni

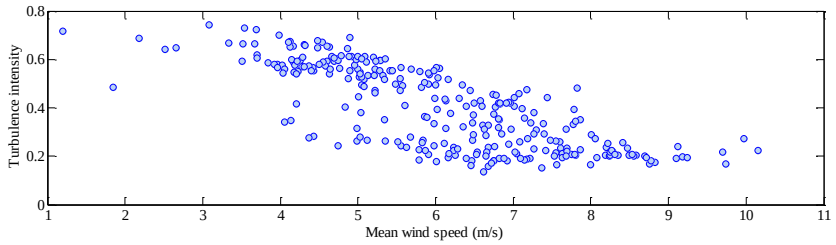

(a) Longitudinal direction

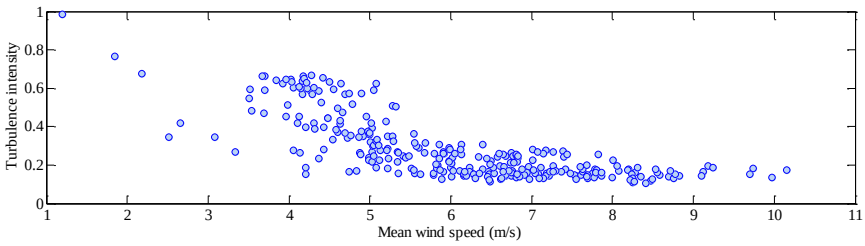

(b) Lateral direction

Fig. 13 Relationship between mean speed and turbulence intensity during Typhoon Chan-hom

I_i (i=u,v) and the gust factor G_i (i=u,v) in the longitudinal and lateral directions can be defined as:

$$I_i = \frac{\sigma_i}{U} \quad (i = u, v) \tag{5}$$

$$G_u = 1 + \frac{\max(\bar{u}_{t_g})}{U} \tag{6}$$

$$G_v = \frac{\max(\bar{v}_{t_g})}{U} \tag{7}$$

where σ_u and σ_v are the root mean square (RMS) values of the turbulence component in the longitudinal and lateral directions, respectively; and U is the 10-min mean wind speed in the longitudinal direction. In this study, we choose t_g=3 s as the duration of the gust wind; $\bar{u}_x(t_g)$ and $\bar{u}_y(t_g)$ are the longitudinal and lateral average wind speeds within the 3 s interval, respectively.

Fig. 12 shows the variations of the turbulence intensities in the longitudinal and lateral directions in the 10-min interval, measured by the two anemometers (UAN_L6 and ANE_L35) during Typhoon Goni. It is observed from Fig. 12 that the values of the turbulence intensities measured by the two anemometers (UAN_L6 and ANE_L35) are varied with time with a similar tendency and reach a peak value around 15:00 on 24 August 2015. The average values of the longitudinal and lateral turbulence intensities of Typhoon Goni are 0.397 and 0.291, respectively, and the maximum values are 0.789 and 0.786, respectively. Fig. 13 demonstrates the relationship between the average wind speed and the turbulence intensity, measured by the ultrasonic anemometer UAN_L6 during Typhoon Chan-hom. It is obviously seen from Fig. 13 that the turbulence intensity is decreased with the increase of the average wind speed. Furthermore, the 10-min turbulence intensities during three typhoons are also calculated and used to facilitate the comparative study. Table 1 and Table 2 give

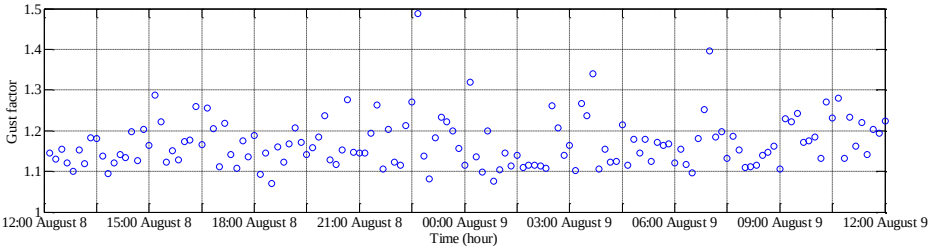

(a) Longitudinal direction

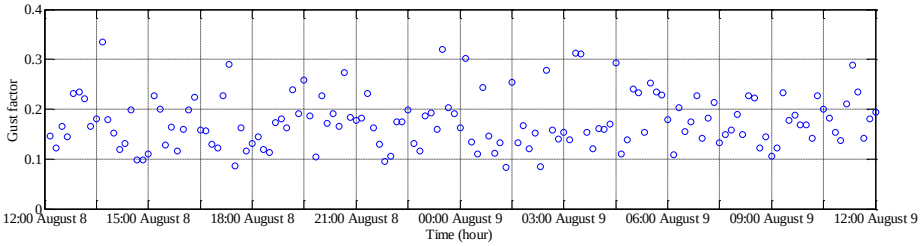

(b) Lateral direction

Fig. 14 Gust factor during Typhoon Soudelor

Table 1 Maximum values of turbulence intensity during three typhoons

Typhoon	Longitudinal I_u	Lateral I_v
Typhoon Chan-hom	0.7418	0.9844
Typhoon Soudelor	0.4019	0.2401
Typhoon Goni	0.7890	0.7868

Table 2 Mean values of turbulence intensity during three typhoons

Typhoon	Longitudinal $\bar{I}_u$	Lateral $\bar{I}_v$	$\bar{I}_v/\bar{I}_u$
Typhoon Chan-hom	0.3628	0.2719	0.74945
Typhoon Soudelor	0.1397	0.1309	0.93682
Typhoon Goni	0.3965	0.2918	0.74359

the maximum and mean values of the turbulence intensity. The mean turbulence intensity of Typhoon Goni is larger than others in both the longitudinal and lateral directions.

Fig. 14 presents the values of the longitudinal and lateral gust factors in the 10-min interval, measured by the ultrasonic anemometers UAN_L6 during Typhoon Soudelor. The average values of the longitudinal and lateral gust factors are 1.184 and 0.198, respectively. The ratio of the gust factors of the two components is G_u:G_v=1:0.167.

3.3 Turbulence integral scale

Based on the derived wind speed and direction in the 10-min interval, the turbulence integral scale can be calculated by use of the auto-correlation function integral method as expressed by (Simiu and Scanlan 1996)

$$L_i^x = \frac{U}{\sigma_i^2}\int_0^\infty R_i(\tau)d\tau \qquad (i=u,v) \tag{8}$$

where U is the average wind speed; σ_i is the standard deviation of the turbulent components; and $R_i(\tau)$ represents the auto-correlation function of the fluctuating wind.

The mean values of the 10-min turbulence integral scale during three typhoons are shown in Table 3. Taking Typhoon Soudelor as an example, the turbulence integral scales of the fluctuating wind are 206.72 m and 124.90 m in the along-wind and cross-wind directions, respectively. However, the turbulence integral scales of Typhoon Chan-hom and Typhoon Goni are far less than that of Typhoon Soudelor. Because the mean wind speeds of Typhoon Chan-hom and Typhoon Goni are much smaller than that of Typhoon Soudelor. Fig. 15 shows the histograms of 10-min turbulence integral scale of Typhoon Soudelor. It can be found from Fig. 15 that the along-wind turbulence integral scales are mostly distributed in the range from 50 m to 300 m and the most proportion of the turbulence integral scale is around 110 m. With respect to the across-wind turbulence integral scales, the concentration domain is ranged from 50 m to 100 m and the peak area is located around 70 m.

Table 3 Mean values of 10-min turbulence integral scale of three typhoons (m)

Typhoon	Typhoon Chan-hom	Typhoon Soudelor	Typhoon Goni
Along-wind (L_u)	89.2908	206.7202	58.1865
Across-wind (L_v)	46.6108	124.8991	37.6344

3.4 Power spectral density

The energy distribution of the fluctuating wind can be expressed in the form of the power spectral density (PSD). In this study, several along-wind spectra including Karman spectrum (Von Karman 1948), Kaimal spectrum (Kaimal *et al.* 1972), and Teunissen spectrum (Teunissen 1980) are adopted to compare the PSD of turbulence in the along-wind direction. These spectra are defined as:

Karman spectrum

$$\frac{nS_u(Z,n)}{(u^*)^2} = \frac{4\beta f}{(1+70.8f^2)^{5/6}} \tag{9}$$

$$f = nL_u^x/U \tag{10}$$

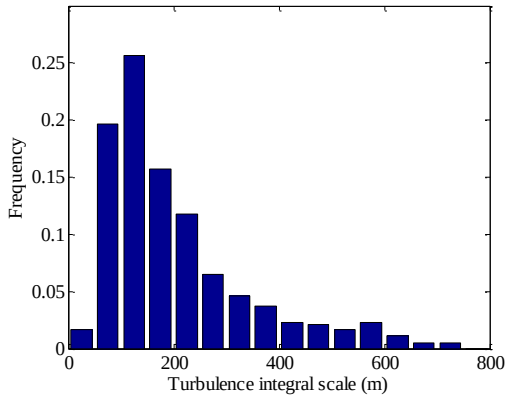

(a) Along-wind

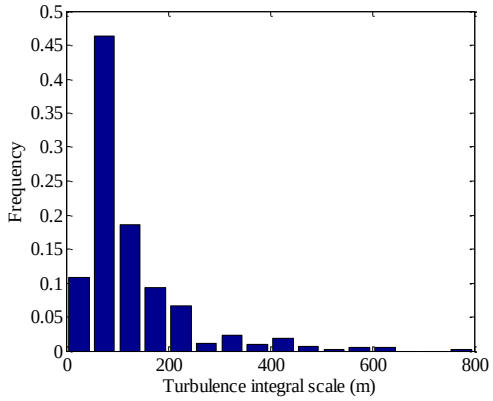

(b) Across-wind

Fig. 15 Histograms of turbulence integral scale

Table 4 Values of fiction wind speed

Typhoon	Typhoon Chan-hom	Typhoon Soudelor	Typhoon Goni
u^*	0.6248	0.2346	0.6545

$$\sigma_u^2 = \beta (u^*)^2 \tag{11}$$

Kaimal spectrum

$$\frac{nS_u(Z,n)}{(u^*)^2} = \frac{200f}{(1+50f)^{5/3}} \tag{12}$$

$$f = nZ/U \tag{13}$$

Teunissen spectrum

$$\frac{nS_u(Z,n)}{(u^*)^2} = \frac{105f}{(0.44+33f)^{5/3}} \tag{14}$$

$$f = nZ/U \tag{15}$$

where S_u is the PSD of along-wind turbulence; n is the natural frequency of the fluctuating wind; Z is the altitude of the wind speed; U is the mean speed at the standard height; β is the coefficient of the friction wind speed; σ_u is the standard deviation of the fluctuating wind speed; and u^* is the friction wind speed which can be calculated by the energy unitary method (Simiu and Scanlan 1996) as expressed by

$$(u^*)^2 = \sigma_u^2 / 6 \tag{16}$$

Table 4 lists the friction wind speed values of three typhoons which are different from each other. The friction wind speed value of Typhoon Chan-hon is similar to that of Typhoon Goni.

The PSD of the wind speed is one of the significant factors which affect the wind-induced dynamic responses of long-span bridges, thus it is essential to analyze the PSD function based on the measured wind data. Fig. 16 illustrates a comparison of the measured along-wind turbulence PSD with three typical PSDs of three typhoons. It can be seen from Fig. 16 that the measured along-wind turbulence power densities are basically matched with the selected PSDs. In order to evaluate the matching degree of

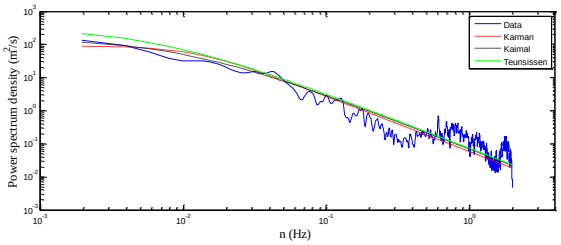

(a) Typhoon Chan-hom

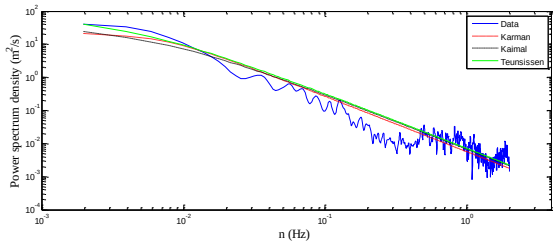

(b) Typhoon Soudelor

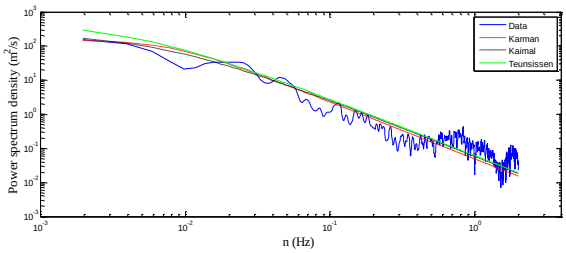

(c) Typhoon Goni

Fig. 16 Along-wind PSD of turbulence during three typhoons

Table 5 RMS value of selected PSD to measured PSD

Typhoon	Karman spectrum	Kaimal spectrum	Teunsissen spectrum
Typhoon Chan-hom	1.65785	0.92074	3.06191
Typhoon Soudelor	0.62854	0.64010	0.29590
Typhoon Goni	1.51966	1.462055	4.37309

each selected PSD to the measured PSD of three typhoons, the RMS values are calculated and listed in Table 5. From Table 5, it can be found that Kaimal spectrum matches well with the measured spectra of Typhoon Chan-hom and

Typhoon Goni, and Teunsissen spectrum matches well with the measured spectrum of Typhoon Soudelor. However, there still has a deviation between the selected spectra and the measured spectrum. Taking Typhoon Soudelor as an example, Teunsissen spectrum matches quite well with the measured spectrum but the range between 0.01 Hz~0.4 Hz of the measured PSD is overestimated. Both Karman spectrum and Kaimal spectrum underestimate the PSD of turbulence in the low-frequency region and overestimate that in the middle region. In the case of Typhoon Chan-hom, the selected PSDs fit well with the measured PSD in the range of low frequency but have a fluctuation in the range of high frequency. As for Typhoon Goni, the measured PSD is overestimated by all the selected PSDs in the low frequency region, while the measured PSD is higher than all selected PSD in the high-frequency ranging from 0.7 Hz to 2 Hz.

4. Probabilistic modeling of wind speed and direction

4.1 Angular-linear model

There are several major approaches for the construction of bivariate distribution. One of these approaches to construct the joint distribution function is based on the univariate PDF, such as the isotropic Gaussian model (McWilliams *et al.* 1979), anisotropic Gaussian model (Weber 1991), Farlie-Gumbel-Morgenstern model (Johnson and Kotz 1975), and angular-linear model (Johnson and Wehrly 1978). In the study, the angular-linear model is adopted to establish the joint probability distribution of the wind speed and direction.

As the name implies, the angular-linear model is used to construct the joint distribution of bivariate random variables when one variable is directional and the other is scalar. The PDF of the angular-linear model is defined as

$$f(\theta,x) = 2\pi g(\delta) f_1(\theta) f_2(x) \tag{17}$$

where $f(\theta,x)$ represents the joint probability distribution of the wind speed and direction; $f_1(\theta)$ denotes the PDF of the wind direction; $f_2(x)$ is the PDF of the wind speed; and $g(\bullet)$ is the PDF of the circular variable δ, defined as

$$\delta = 2\pi[F_1(\theta) - F_2(x)] \tag{18}$$

where $F_1(\theta)$ and $F_2(x)$ represent the CDF of the wind direction and wind speed, respectively.

To construct the joint bivariate distribution of the wind speed and direction by use of the angular-linear approach, the univariate marginal distributions of the wind speed and direction should be determined. In the literatures, several distributions were used to model the wind speed, including Weibull distribution, Frechet distribution, and Gumbel distribution. In this study, a two-parameter Weibull distribution is selected to model the wind speed (Seguro and Lambert 2000), which is defined as

$$f(x;c,k) = k\frac{x^{k-1}}{c^k}\exp(-\frac{x}{c})^k,\ x>0,\ k>0,\ c>0 \tag{19}$$

or

$$F(x;c,k) = 1-\exp[-(\frac{x}{c})^k],\ x>0,\ k>0,\ c>0 \tag{20}$$

where $f(x;c,k)$ and $F(x;c,k)$ represent the PDF and CDF, respectively; and the two key parameters are: $k>0$, the shape parameter, and $c>0$, the scale parameter of the distribution.

For the PDF of the wind direction, the mixture of von Mises distribution is chosen (Carta *et al*. 2008b), which is the most useful continuous probability distribution on the circle for statistical analysis of angular data. The von Mises probability distribution for the angle θ is given by

$$f(\theta;\mu,\kappa) = \frac{1}{2\pi I_0(\kappa)}\exp[\kappa\cos(\theta-\mu)],\ 0\le\theta\le 2\pi \tag{21}$$

or

$$F(\theta;\mu,\kappa) = \int_0^{\theta} f(\theta;\mu,\kappa) \tag{22}$$

where $f(\theta;\mu,\kappa)$ and $F(\theta;\mu,\kappa)$ represent the PDF and CDF, respectively; the parameter μ is a measure of the location which means that the distribution is symmetrically distributed around μ; and the parameter κ is a measure of concentration. Here, $I_0(k)$ is the modified Bessel function of order zero, which is expressed by

$$I_0(k) = \sum_{k=0}^{\infty}\frac{1}{(k!)^2}(\frac{\kappa}{2})^{2k} \tag{23}$$

After obtaining the univariate marginal distributions of the wind speed and direction, the circular variable δ can be calculated by Eq. (18). A mixture of von Mises distribution is chosen to construct the distribution of circular variable δ. The parameter estimation of these three univariate marginal distributions will be described in the following section.

4.2 Parameter estimation

In this study, the EM algorithm is used to estimate the unknown parameters w_i, k_i, c_i (i=1,…,n) in the mixture of Weibull distribution and w_i, μ_i, κ_i (i=1,…,n) in the mixture of von Mises distribution. Since the finite mixture distribution model includes the latent variable, specifying the weight of each component of the mixture model, the EM algorithm is a useful tool for finding the maximum likelihood estimation of the mixture parameters (McLachlan and Basford 1998).

The EM algorithm, which is a method to find a locally maximum likelihood from the incomplete data, can be applied to find the maximum likelihood parameters of a statistical model in the case where the equations cannot be solved directly. The EM algorithm estimates the parameters by a way to solve two sets of equations numerically namely E-step and M-step. For example, given the statistical model which generates a set **x** of observed data, a set of latent data **Z**, and a vector of unknown parameters **θ**, the flowchart of the EM algorithm is shown in Fig. 17, and the EM algorithm estimate the parameters by the following two steps:

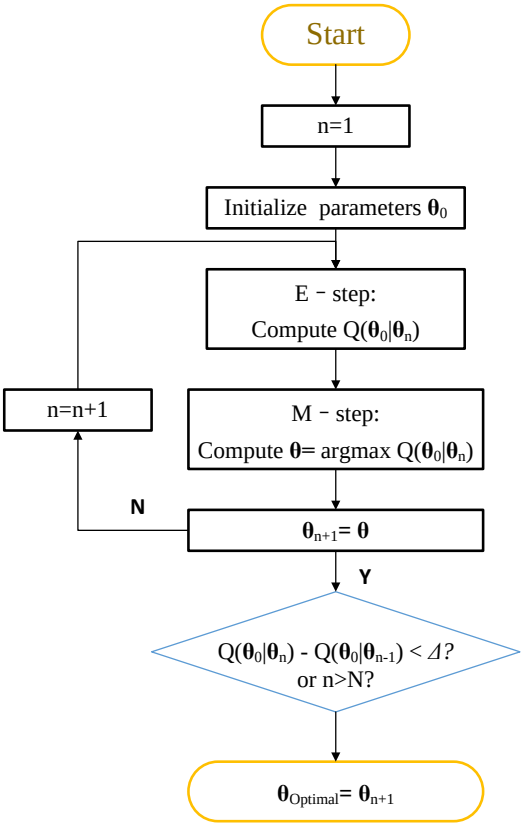

Fig. 17 Flowchart of EM method

(1) Expectation step (E-step): compute the conditional expectation value of the logarithm likelihood function

$$Q(\boldsymbol{\theta}|\boldsymbol{\theta}^{(t)}) = E[\log\, p(\mathbf{Z},\mathbf{x}|\boldsymbol{\theta})|\mathbf{x},\boldsymbol{\theta}^{(t)}] \tag{24}$$

(2) Maximization step (M-step)

$$\boldsymbol{\theta}^{(t+1)} = \arg\max_{\theta} Q(\boldsymbol{\theta}|\boldsymbol{\theta}^{(t)}) \tag{25}$$

As for the wind speed distribution, the mixture of Weibull distribution can be expressed by

$$f(v|w_k,c_k,k_k) = \sum_{k=1}^{K} w_k k_k \frac{v^{k_k-1}}{c_k^{\,k_k}} \exp(-\frac{v}{c_k})^{k_k} \tag{26}$$

where w_k, k_k, c_k are the weight and parameters of the Weibull distribution. The detailed procedure about the parameter estimation of the wind speed distribution by the EM algorithm is described as follows:

(1) Initialize the parameters w_k^0, k_k^0, c_k^0 (k=1,…, K) in the mixture of Weibull distribution randomly;

(2) Expectation step: the responsibility γ_{ik} of the component k for the wind speed sample x_i can be estimated using the current parameter values as expressed

$$\gamma_{ik} = \frac{w_k f(x_i|c_k,k_k)}{\sum_{k=1}^{K} w_k f(x_i|c_k,k_k)} \tag{27}$$

(3) Maximization step: the new values of parameters w_k, k_k, c_k are calculated by

$$w_k = \frac{1}{n}\sum_{i=1}^{n}\gamma_{ik} \tag{28}$$

The values of k_k are given as the roots of the function

$$f(k_k) = \frac{1}{k_k} + \frac{\sum_{i=1}^{n}\gamma_{ik}\ln(x_i)}{\sum_{i=1}^{n}\gamma_{ik}} - \frac{\sum_{i=1}^{n}\gamma_{ik}x_i^{k_k}\ln(x_i)}{\sum_{i=1}^{n}\gamma_{ik}x_i^{k_k}} \tag{29}$$

$$c_k = \left(\frac{\sum_{i=1}^{n}\gamma_{ik}x_i^{k_k}}{\sum_{i=1}^{n}\gamma_{ik}}\right)^{\frac{1}{k_k}} \tag{30}$$

As for the wind direction distribution, the mixture of von Mises distribution can be expressed by

$$f(\theta;w_k,\mu_k,\kappa_k) = \sum_{k=1}^{K}\frac{w_k}{2\pi I_0(\kappa_k)}\exp[\kappa_k\cos(x-\mu_k)] \tag{31}$$

where w_k, μ_k, κ_k are the weight and parameters of the von Mises distribution. Presented in the following is the framework for estimating the parameters of the wind direction distribution by the EM algorithm which is derived in Calderara *et al.* (2011) and the method to determine the initial parameters w_k^0, μ_k^0, κ_k^0 as addressed in Heckenbergerova *et al.* (2015).

(1) Initial step: in order to obtain the initial values, the entire wind direction range is divided into K parts, and the initial weight for each interval w_k^0 (k=1,…, K) is given by relative observation data.

$$w_k^0 = \frac{\sum_{L_i}^{Ui} X_i}{n} \tag{32}$$

where L_i and U_i are the boundaries of the i^{th} interval; and n is the total number of data.

The concentration parameters μ_k^0 are estimated by:

$$\mu_k^0 = \begin{cases} \arctan\dfrac{s_k}{c_k} + \pi & \text{if} \quad c_k < 0 \\ \arctan\dfrac{s_k}{c_k} & \text{if} \quad s_k > 0 \cup c_k > 0 \\ \arctan\dfrac{s_k}{c_k} + 2\pi & \text{if} \quad s_k < 0 \cup c_k > 0 \end{cases} \tag{33}$$

where

$$c_k = \frac{\sum_{i=1}^{n}\cos(\theta_i)}{n_k}, \quad s_k = \frac{\sum_{i=1}^{n}\sin(\theta_i)}{n_k} \tag{34}$$

The initial values of the concentration parameters κ_k^0 are evaluated as the roots of the function

$$\frac{I_1(\kappa_k^0)}{I_0(\kappa_k^0)} = \sqrt{c_k^2 + s_k^2} \tag{35}$$

(2) Expectation step: the responsibility γ_{ik} of the component k for the wind direction sample θ_i can be estimated using the parameter values of the previous

iteration as expressed by

$$\gamma_{ik} = \frac{w_k f(\theta_i | \mu_k^0, \kappa_k^0)}{\sum_{s=1}^{K} w_s f(\theta_i | \mu_s^0, \kappa_s^0)} \tag{36}$$

(3) Maximization step: the M step calculates the new values of the mixture parameters $\boldsymbol{w}=\{w_1,\ldots,w_K\}$, $\boldsymbol{\kappa}=\{\kappa_1,\ldots,\kappa_K\}$, $\boldsymbol{\mu}=\{\mu_1,\ldots,\mu_K\}$. They can be estimated for each component k by

$$w_k = \frac{1}{n}\sum_{i=1}^{n}\gamma_{ik} \tag{37}$$

$$\mu_k = \arctan\left(\frac{\sum_{i=1}^{n}\gamma_{ik}\sin\theta_i}{\sum_{i=1}^{n}\gamma_{ik}\cos\theta_i}\right) \tag{38}$$

The values of κ_k are given as roots of function

$$A(\kappa_k) = \frac{I_1(\kappa_k)}{I_0(\kappa_k)} = \frac{\sum_{i=1}^{n}\gamma_{ik}\cos(\theta_i - \theta_0^k)}{\sum_{i=1}^{n}\gamma_{ik}} \tag{39}$$

The Expectation step and Maximization step are iterated until the convergence (reached when the likelihood change in the limit range between two consecutive iterations) or reach a given number of iterations.

4.3 Selection of optimal model

To evaluate if the wind data measured during typhoons match the selected statistical distribution models, the candidate distribution models with different components need to be compared and then selected based on the fit performance. In this study, the R^2 statistic and the AIC value as the fitness performance to select the optimal distribution model are used.

The AIC value is first announced by Akaike in 1974 and is a measure of the relative quality of statistical models for a set of data (Akaike 1974). The AIC value aims to measure the goodness of fit based on the likelihood function. The AIC value of the model is expressed by

$$\mathrm{AIC} = 2k - 2\ln(L) \tag{40}$$

where L is the value of the maximum likelihood function of the model; and k is a penalty which is the number of estimated parameters in the model. This penalty discourages overfitting and increases the value of AIC with the increase of estimated parameter number. It can be found that the lower AIC value is, the better model is.

In statistics, the coefficient of determination denoted R^2 improves a measure of how well the observed outcomes are replicated by the distribution model. R^2 statistic is a special bin test and it focuses on measuring the fit performance between the expected and observed frequencies of the bins. The most general definition of the R^2 statistic is expressed as

$$R^2 = 1 - \frac{SS_{res}}{SS_{tot}} \tag{41}$$

The term SS_{tot} denotes the total sum of squares which shows the proportional to the variance of the data. It is defined as the sum of the squared differences between the observed and average frequency of all bins.

$$SS_{tot} = \sum_i (y_i - \bar{y})^2 \tag{42}$$

The term SS_{res} denotes the sum of squares of residuals which reflects the total discrepancy between the observed data and the estimation model.

$$SS_{res} = \sum_i (y_i - f_i)^2 = \sum_i e_i^2 \tag{43}$$

It is obvious that the value of R^2 statistic is between zero and one, and the higher R^2 value is, the more likely the measured data match the distribution model.

4.4 Application to Jiubao Bridge

In order to demonstrate the effectiveness of the above-mentioned procedure in bivariate modeling, the wind monitoring data of the Jiubao Bridge during typhoons are employed for the construction of the joint distribution of the wind speed and direction. In consideration of the effect of heavy rain on the normality of the ultrasonic anemometer during typhoons, the wind data measured by the mechanical anemometer ANE_L4 are chosen for further analysis.

As described in the previous section, the angular-linear joint distribution model depends on the construction of

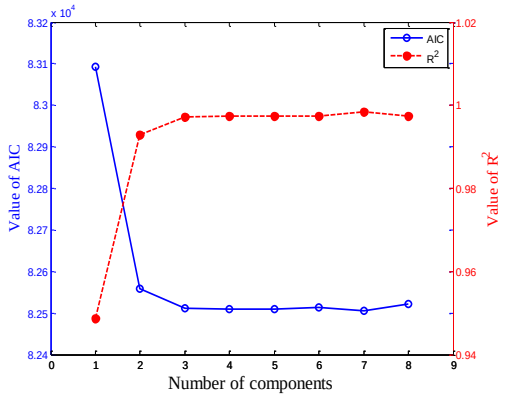

(a) AIC and R^2 values

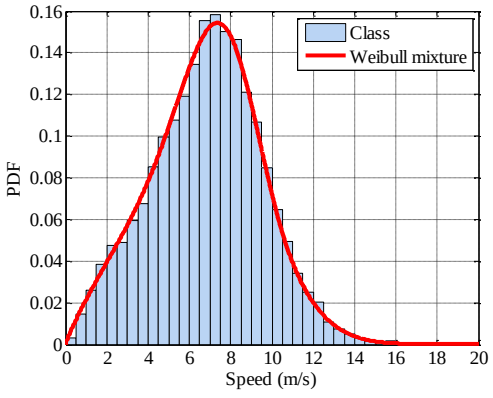

(b) Histogram and PDF of wind speed

Fig. 18 Distribution model of wind speed

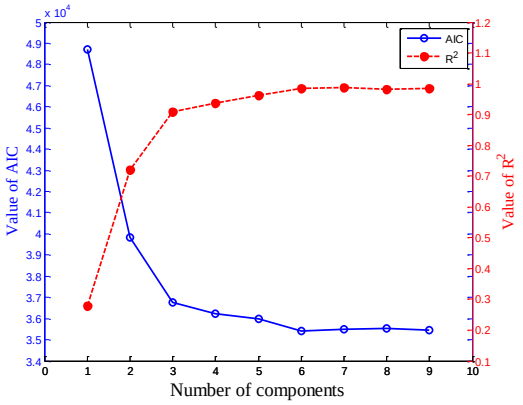

(a) AIC and R^2 values

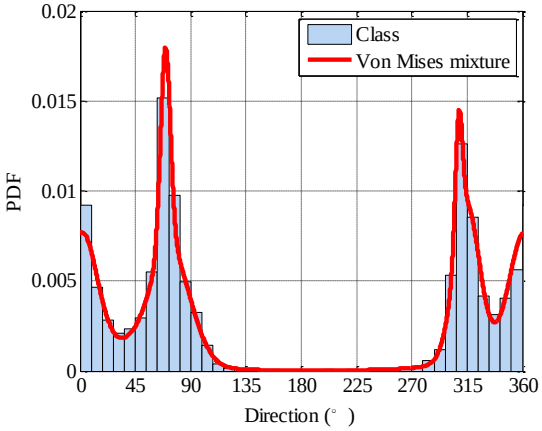

(b) Histogram and PDF of wind speed

Fig. 19 Distribution model of wind direction

three univariate distribution models, i.e., the wind speed distribution model, the wind direction distribution model, and the circular variable distribution model. Thus, the first step is to construct the univariate distribution of the wind speed and direction and estimate the parameters of each distribution by the EM method. The next step is to calculate the circular variable and construct the distribution of the circular variable. For each univariate distribution model, the AIC and R^2 are used to evaluate the fitness performance of each model and choose the optimal model. After that, the joint PDF of the wind speed and direction can be obtained.

In this study, the Weibull distribution is chosen for the construction of the wind speed model and the EM method is adopted to estimate the parameters of the model, i.e., w_i, k_i and c_i. For this purpose, the wind speed spectrum ranging from 0 m/s to 20 m/s is divided into 40 bins with an equal width, and the corresponding probability densities are calculated. Based on these probability densities, the parameters of the wind speed mode with different components are estimated. Fig. 18 shows the values of AIC and R^2 with different numbers of components of the wind speed. It is obviously observed from Fig. 18 that, for the wind speed data, the values of AIC and R^2 become stable from three components. This means that a mixture Weibull distribution with three components is sufficient to model the wind speed distribution, and the parameters of the optimal model are listed in Table 6.

Table 6 Estimated parameters of angular-linear model

Distribution		Value of parameter		
Wind speed	Weibull distribution	Weight (w)	Scale parameter (c) (m/s)	Shape parameter (k)
		0.3332	7.85599	4.73984
		0.3332	8.83756	3.57578
		0.3336	5.95338	1.88789
Wind direction	Von Mises distribution	Weight (w)	Location parameter (μ) (rad)	Concentration parameter (κ)
		0.1880	0.02828	22.86277
		0.1124	1.21237	207.71978
		0.2569	1.27857	12.60357
		0.1741	0.17767	1.88044
		0.0486	5.37936	403.47627
		0.2200	5.49044	31.23524
Circular variable	Von Mises distribution	Weight (w)	Location parameter (μ) (rad)	Concentration parameter (κ)
		0.2094	0.53505	3.41286
		0.1737	1.72808	3.62675
		0.1315	2.85067	5.68220
		0.1214	3.76685	4.23272
		0.1266	4.82119	3.19768
		0.2374	5.78352	3.61949

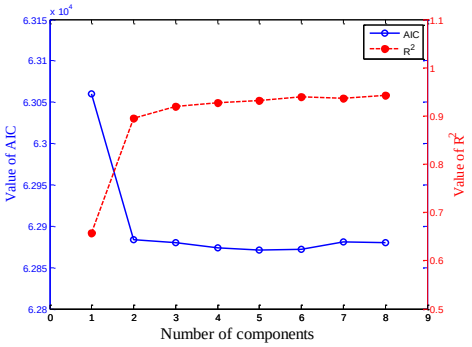

(a) AIC and R^2 values

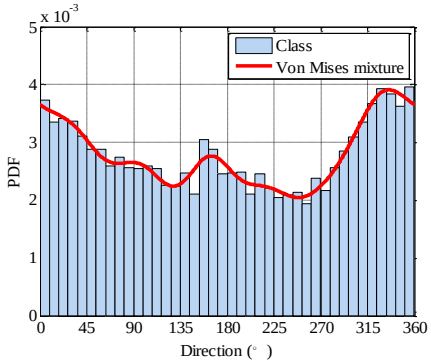

(b) Histogram and PDF of wind speed

Fig. 20 Distribution model of circular variable

For the wind direction distribution, the von Mises distribution is used to construct the wind direction model. Similarly, 40 bins spanning the whole wind direction range

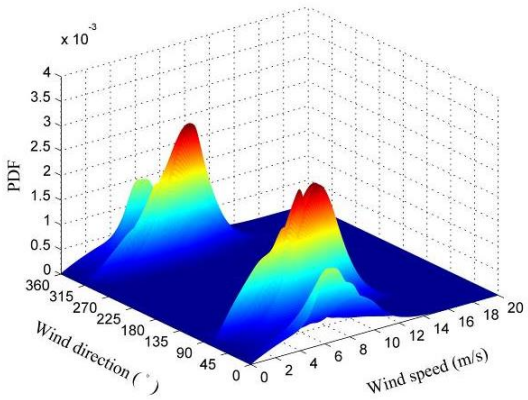

(a) Fitted AL joint distribution model

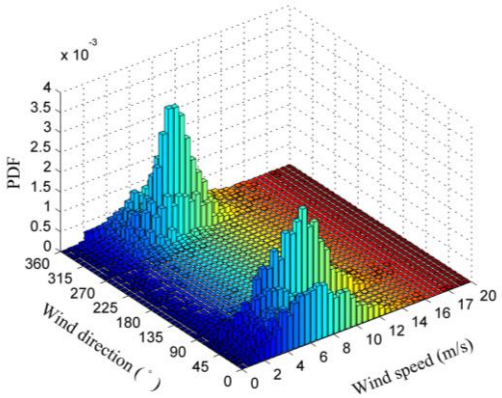

(b) Histogram of wind speed and direction

Fig. 21 Joint distribution model of Typhoon Chan-hom

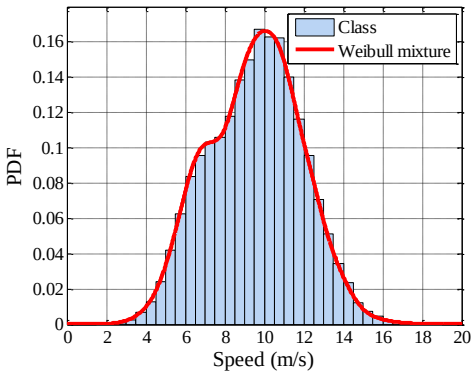

(a) Histogram and PDF of wind speed

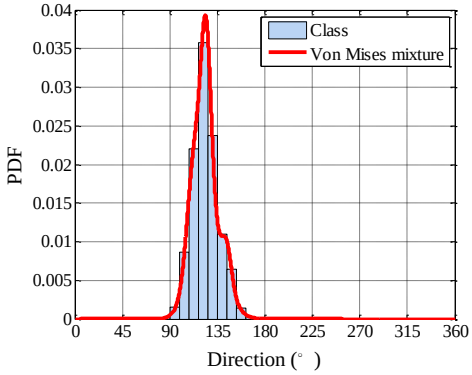

(b) Histogram and PDF of wind direction

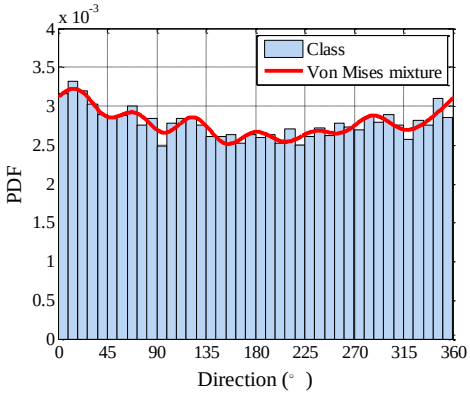

(c) Histogram and PDF of circular variable

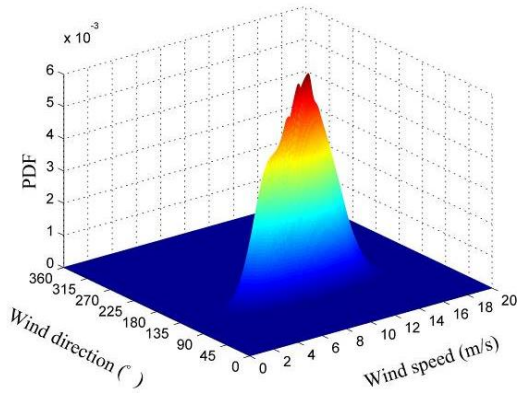

(d) Fitted AL joint distribution model

Fig. 22 Joint distribution model of Typhoon Soudelor

with an equal width are calculated and these probabilities are applied to estimate the parameters. The values of AIC and R^2 with different numbers of components of the wind direction is illustrated in Fig. 19. The values of AIC and R^2 is stable from six components which means that the increase of components cannot generate better performance of the wind direction model. Thus, the mixture of von Mises distribution with six components is regarded as the optimal wind direction distribution model, and the parameters of the optimal model are listed in Table 6.

After obtaining the parameters relative to the angular and linear component of the model, the next step is to combine these two components for the construction of a joint distribution function to fit the profile of the wind speed and direction simultaneously. The same statistical analysis procedure is applied to model the circular variable, as shown in Fig. 20, and the values of AIC and R^2 become stable from six components. Then, the mixture of von Mises distribution with six components is regarded as the circular variable distribution model, and the parameters of the optimal model are listed in Table 6.

Finally, three optimal univariate distribution models are determined and the parameters of each distribution are estimated. Then, the overall joint PDF of the wind speed and direction can be derived as shown in Fig. 21(a), and the histogram of the wind speed and direction is illustrated in

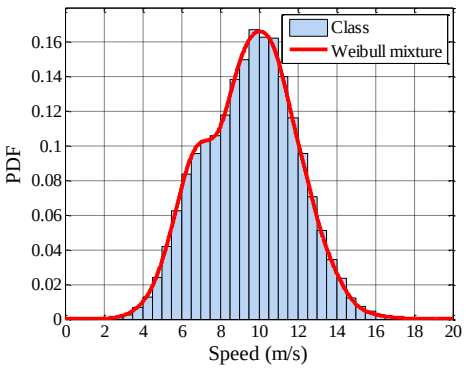

(a) Histogram and PDF of wind speed

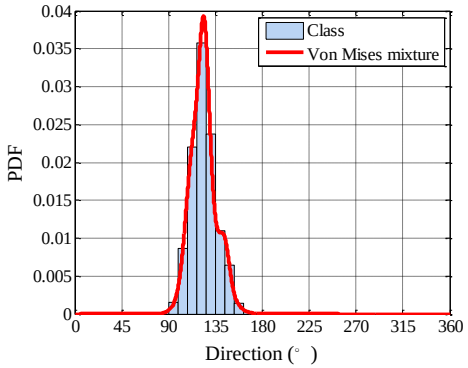

(b) Histogram and PDF of wind direction

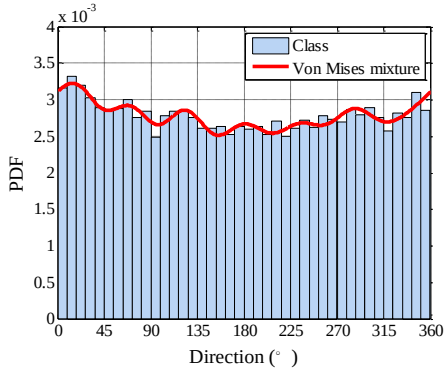

(c) Histogram and PDF of circular variable

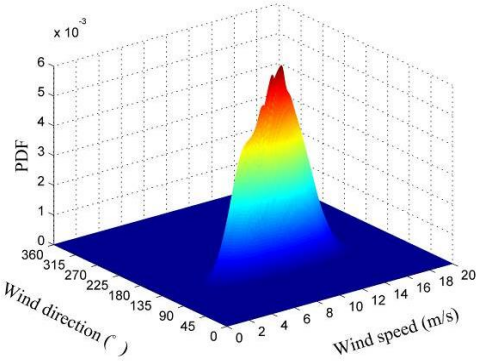

(d) Fitted AL joint distribution model

Fig. 23 Joint distribution model of Typhoon Goni

Fig. 21(b).

Likewise, the measured wind data of Typhoon Soudelor and Typhoon Goni are used to construct the joint distribution models by the angular-linear approach. Fig. 22 shows the calculated joint distribution of the wind speed and direction for the wind data of Typhoon Soudelor, which includes the histogram and PDF of the wind speed (Fig. 22(a)), the histogram and PDF of the wind direction (Fig. 22(b)), the histogram and PDF of the circular variable (Fig. 22(c)), and the joint PDF of the wind speed and direction (Fig. 22(d)). In the same way, the result of the joint distribution of Typhoon Goni is shown in Fig. 23.

5. Conclusions

This paper addressed the statistical analysis of the wind characteristics during typhoons and the bivariate probabilistic modeling of the wind speed and direction by the proposed EM algorithm-based angular-linear modeling approach using long-term wind monitoring data of the arch Jiubao Bridge located in Hangzhou, China. The wind characteristics nearby the bridge site recorded by the SHM system instrumented on the bridge were presented and carefully examined. Then, the measured wind data are adopted to construct the joint PDF of the wind speed and direction by use of the proposed EM algorithm-based angular-linear approach. For the angular-linear modeling approach, the distribution model of the wind speed and the wind direction were firstly obtained respectively and then the joint distribution model of the wind speed and direction was formulated by the circular variable. The finite mixture of Weibull distribution and the mixture of von Mises distribution were used to represent the wind speed distribution and the wind direction distribution, respectively. The EM algorithm-based unknown parameter estimation method was employed to estimate the parameters in the finite mixture distribution models, and the optical model was determined by the values of R^2 statistic and AIC.

The obtained results demonstrate that: (i) the stochastic properties of the wind field at the bridge site measured by the SHM system during typhoons are effectively characterized by the proposed EM algorithm-based angular-linear modeling approach; (ii) the mixture of Weibull distribution and the mixture of von Mises distribution have a favorable performance in modeling the distribution of the wind speed and the wind direction, respectively; (iii) the joint PDF of the wind speed and direction constructed by the angular-linear approach can reflect the multimodal characteristic and consider the correlation between the wind speed and direction; and (iv) the results of statistical analysis and probabilistic modeling of the wind characteristics can facilitate the structural performance evaluation of the bridge under the typhoon attack as well as the prediction of typhoon-induced fatigue damage of the critical structural components on the bridge.

Acknowledgments

The work described in this paper was jointly supported by the National Science Foundation of China (Grant No.

51778574), the Fundamental Research Funds for the Central Universities of China (Grant No. 2017QNA4024), and the Key Lab of Structures Dynamic Behavior and Control (Harbin Institute of Technology), Ministry of Education of the PRC.

References

Akaike, H. (1974), "A new look at the statistical model identification", *IEEE T. Automat. Contr.*, **19**(6), 716-723.

Alduse, B.P., Jung, S., Vanli, O.A. and Kwon, S.D. (2015), "Effect of uncertainties in wind speed and direction on the fatigue damage of long-span bridges", *Eng. Struct.*, **100**, 468-478.

Bietry, J., Delaunay, D. and Conti, E. (1995), "Comparison of full-scale measurement and computation of wind effects on a cable-stayed bridge", *J. Wind Eng. Ind. Aerod.*, **57**(2), 225-235.

Cai, C.S., Hu, J., Chen, S., Han, Y., Zhang, W. and Kong, X. (2015), "A coupled wind-vehicle-bridge system and its applications: a review", *Wind Struct.*, **20**(2), 117-142.

Calderara, S., Prati, A. and Cucchiara, R. (2011), "Mixtures of von mises distributions for people trajectory shape analysis", *IEEE T. Circ. Syst. Vid.*, **21**(4), 457-471.

Carta, J.A., Ramirez, P. and Bueno, C. (2008a), "A joint probability density function of wind speed and direction for wind energy analysis", *Energ. Convers. Manage.*, **49**(6), 1309-1320.

Carta, J.A., Bueno, C. and Ramirez, P. (2008b), "Statistical modelling of directional wind speeds using mixtures of von Mises distributions: Case study", *Energ. Convers. Manage.*, **49**(5), 897-907.

Chen, B., Yang, Q.S., Wang, K. and Wang, L.N. (2013), "Full-scale measurements of wind effects and modal parameter identification of Yingxian wooden tower", *Wind Struct.*, **17**(6), 609-627.

Cheng, J. and Li, Q.S. (2009), "Reliability analysis of long span steel arch bridges against wind-induced stability failure", *J. Wind Eng. Ind. Aerod.*, **97**(3), 132-139.

Coles, S.G. and Walshaw, D. (1994), "Directional modelling of extreme wind speeds", *Appl. Stat.*, 139-157.

Comanducci, G., Ubertini, F. and Materazzi, A.L. (2015), "Structural health monitoring of suspension bridges with features affected by changing wind speed", *J. Wind Eng. Ind. Aerod.*, **141**, 12-26.

Ding, Y.L., Song, Y.S., Cao, B.Y., Wang, G.X. and Li, A.Q. (2016), "Full-range S-N fatigue-life evaluation method for welded bridge structures considering hot-spot and welding residual stress", *J. Bridge Eng. - ASCE*, **21**(12), 04016096.

Ding, Y.L., Zhao, H.W. and Li, A.Q. (2017), "Temperature effects on strain influence lines and dynamic load factors in a steel-truss arch railway bridge using adaptive FIR filtering", *J. Perform. Constr. Fac. - ASCE*, doi: 10.1061/(ASCE)CF.1943-5509.0001026.

Erdem, E. and Shi, J. (2011), "Comparison of bivariate distribution construction approaches for analysing wind speed and direction data", *Wind Energy*, **14**(1), 27-41.

Ge, Y.J. and Xiang, H.F. (2002), "Statistical study for mean wind velocity in Shanghai area", *J. Wind Eng. Ind. Aerod.*, **90**(12), 1585-1599.

Ge, Y.J. and Xiang, H.F. (2008), "Recent development of bridge aerodynamics in China", *J. Wind Eng. Ind. Aerod.*, **96**(6), 736-768.

Google Maps (2016), www.google.com.hk/maps/.

Gu, M., Xu, Y.L., Chen, L.Z. and Xiang, H.F. (1999), "Fatigue life estimation of steel girder of Yangpu cable-stayed bridge due to buffeting", *J. Wind Eng. Ind. Aerod.*, **80**(3), 383-400.

Heckenbergerova, J., Musilek, P. and Kromer, P. (2015), Optimization of wind direction distribution parameters using particle swarm optimization, In Afro-European Conference for Industrial Advancement, Springer International Publishing.

Japan Meteorological Agency (2015), http://www.jma.go.jp/jma/jma-eng/jma-center/rsmc-hp-pub-eg/besttrack_viewer_2010s.html.

Johnson, N.L. and Kott, S. (1975), "On some generalized Farlie-Gumbel-Morgenstern distributions", *Commun. Stat. - Theor. M.*, **4**(5), 415-427.

Johnson, R.A. and Wehrly, T.E. (1978), "Some angular-linear distributions and related regression models", *J. Am. Stat. Assoc.*, **73**(363), 602-606.

Kaimal, J.C., Wyngaard, J., Izumi, Y. and Cote, O.R. (1972), "Spectral characteristics of surface - layer turbulence", *Q. J. Roy. Meteor. Soc.*, **98**(417), 563-589.

Lei, Y., Wang, H.F. and Shen, W.A. (2012), "Update the finite element model of Canton Tower based on direct matrix updating with incomplete modal data", *Smart Struct. Syst.*, **10**(4-5), 471-483

Lei, Y., Chen, F. and Zhou, H. (2015), "An algorithm based on two-step Kalman filter for intelligent structural damage detection", *Struct. Control Health Monit.*, **22**(4), 694-706.Li, J., Peng, Y.B. and Yan, Q. (2013), "Modeling and simulation of fluctuating wind speeds using evolutionary phasespectrum", *Probabilist. Eng. Mech.*, **32**, 48-55.

Li, Q.S., Xiao, Y.Q., Wu, J.R., Fu, J.Y. and Li, Z.N. (2008), "Typhoon effects on super-tall buildings", *J. Sound Vib.*, **313**(3), 581-602.

Li, Z.X., Chan, T.H.T. and Ko, J.M. (2002), "Evaluation of typhoon induced fatigue damage for Tsing Ma Bridge", *Eng. Struct.*, **24**(8), 1035-1047.

McLachlan, G.J. and Basford, K.E. (1988), Mixture models. Inference and applications to clustering, Statistics: Textbooks and Monographs, New York.

McWilliams, B., Newmann, M.M. and Sprevak, D. (1979), "The probability distribution of wind velocity and direction", *Wind Eng.*, **3**(4), 269-273.

Ni, Y.Q., Ye, X.W. and Ko, J.M. (2010), "Monitoring-based fatigue reliability assessment of steel bridges: analytical model and application", *J. Struct. Eng. - ASCE*, **136**(12), 1563-1573.

Ni, Y.Q., Ye, X.W. and Ko, J.M. (2012), "Modeling of stress spectrum using long-term monitoring data and finite mixture distributions", *J. Eng. Mech. - ASCE*, **138**(2), 175-183.

Qu, X. and Shi, J. (2010), "Bivariate modeling of wind speed and air density distribution for long-term wind energy estimation", *Int. J. Green Energy*, **7**(1), 21-37.

Simiu, E. and Scanlan, R.H. (1996), Wind effects on structures, John Wiley and Sons, New York

Seguro, J.V. and Lambert, T.W. (2000), "Modern estimation of the parameters of the Weibull wind speed distribution for wind energy analysis", *J. Wind Eng. Ind. Aerod.*, **85**(1), 75-84.

Teunissen, H.W. (1980), "Structure of mean winds and turbulence in the planetary boundary layer over rural terrain", *Bound.-Lay. Meteorol.*, **19**(2), 187-221.

Von Karman, T. (1948), "Progress in the statistical theory of turbulence", *P. Natl. Acad. Sci.*, **34**(11), 530-539.

Wang, L.J., McCullough, M. and Kareem, A. (2013), "A data-driven approach for simulation of full-scale downburst wind speeds", *J. Wind Eng. Ind. Aerod.*, **123**, 171-190.

Weber, R. (1991), "Estimator for the standard deviation of wind direction based on moments of the Cartesian components", *J. Appl. Meteorol.*, **30**(9), 1341-1353.

Xu, Y.L., Liu, T.T. and Zhang, W.S. (2009), "Buffeting-induced fatigue damage assessment of a long suspension bridge", *Int. J. Fatigue*, **31**(3), 575-586.

Xu, Y.L., Zhu, L.D., Wong, K.Y. and Chan, K.W.Y. (2000),

"Field measurement results of Tsing Ma suspension bridge during Typhoon Victor", *Struct. Eng. Mech.*, **10**(6), 545-559.
Xu, Y.L. and Chen, J. (2004), "Characterizing nonstationary wind speed using empirical mode decomposition", *J. Struct. Eng. - ASCE*, **130**(6), 912-920.
Yan, Q., Peng, Y.B. and Li, J. (2013), "Scheme and application of phase delay spectrum towards spatial stochastic wind fields", *Wind Struct.*, **16**(5), 433-455.
Ye, X.W., Ni, Y.Q., Wong, K.Y. and Ko, J.M. (2012), "Statistical analysis of stress spectra for fatigue life assessment of steel bridges with structural health monitoring data", *Eng. Struct.*, **45**, 166-176.
Ye, X.W., Ni, Y.Q., Wai, T.T., Wong, K.Y., Zhang, X.M. and Xu, F. (2013), "A vision-based system for dynamic displacement measurement of long-span bridges: algorithm and verification", *Smart Struct. Syst.*, **12**(3-4), 363-379.
Ye, X.W., Su, Y.H. and Han, J.P. (2014), "Structural health monitoring of civil infrastructure using optical fiber sensing technology: A comprehensive review", *Sci. World J.*, **2014**, Article ID 652329, 1-11.
Ye, X.W., Yi, T.H., Dong, C.Z., Liu, T. and Bai, H. (2015), "Multi-point displacement monitoring of bridges using a vision-based approach", *Wind Struct.*, **20**(2), 315-326.
Ye, X.W., Dong, C.Z. and Liu, T. (2016a), "Force monitoring of steel cables using vision-based sensing technology: methodology and experimental verification", *Smart Struct. Syst.*, **18**(3), 585-599.
Ye, X.W., Su, Y.H., Xi, P.S., Chen, B. and Han, J.P. (2016b), "Statistical analysis and probabilistic modeling of WIM monitoring data of an instrumented arch bridge", *Smart Struct. Syst.*, **17**(6), 1087-1105.
Ye, X.W., Yi, T.H., Dong, C.Z. and Liu, T. (2016c), "Vision-based structural displacement measurement: system performance evaluation and influence factor analysis", *Measurement*, **88**, 372-384.
Ye, X.W., Dong, C.Z. and Liu, T. (2016d), "Image-based structural dynamic displacement measurement using different multi-object tracking algorithms", *Smart Struct. Syst.*, **17**(6), 935-956.